Catalysis Today 171 (2011) 281–289

Contents lists available at ScienceDirect

Catalysis Today

journal homepage: www.elsevier.com/locate/cattod

Catalytic hollow fibre membrane micro-reactor: High purity H_2 production by WGS reaction

F.R. García-García[a], M.A. Rahman[a], I.D. González-Jiménez[b], K. Li[a,*]

[a] Department of Chemical Engineering and Chemical Technology, Imperial College London, London SW7 2AZ, UK
[b] Inorganic Chemistry and Catalysis, Debye Institute for Nanomaterial Science, Utrecht University, Sorbonelaan 16, Utrecht 3584 CA, The Netherlands

ARTICLE INFO

Article history:
Received 30 October 2010
Received in revised form 5 March 2011
Accepted 29 March 2011
Available online 31 May 2011

Keywords:
Asymmetric Al_2O_3 hollow fibre
CuO/CeO_2 catalysts
Water-gas shift reaction
Catalytic hollow fibre membrane micro-reactor

ABSTRACT

In this study, CuO/CeO_2 catalysts with a Cu content ranging from 5% to 40% were synthesized by sol–gel Pechini method and were tested in a fixed-bed reactor for water gas shift (WGS) reaction. The catalysts were characterized by XRD, N_2 adsorption isotherms at 77 K (S_{BET}) and H_2-TPR. Based on the catalytic activity results, 10% CuO/CeO_2, identified to be the most active catalyst, was deposited inside finger-like regions of an Al_2O_3 hollow fibre support for the further development of both catalytic hollow fibre micro-reactor (CHFMR) and catalytic hollow fibre membrane micro-reactor (CHFMMR) where Pd or Pd/Ag membrane was coated on the outer layer of the Al_2O_3 hollow fibre using a single or multilayer electroless plating (ELP) technique. The prepared catalytic membranes were characterized by SEM, EDX, and pure H_2 and Ar permeation. Also, a comparative study of the CO conversion obtained in the WGS reaction as a function of the reaction temperature (from 200 °C to 500 °C) in a fixed-bed reactor, a CHFMR, a Pd-CHFMMR and a Pd/Ag-CHFMMR, was performed showing that the conversion was highest in the Pd/Ag-CHFMMR.

1. Introduction

CO produced in steam reforming of fossil fuels is reoxidised with H_2O to produce more H_2 and CO_2 in water gas shift (WGS) reaction. Both refineries and chemical companies produce H_2 by WGS reaction and use it in desulfurization, hydrotreating and production of chemicals such as NH_3 and CH_3OH. In recent years, because the H_2 has been considered as an energy vector in fuel cell applications, the interest in WGS reactions has increased and new active catalysts have been studied [1]. Among them, the $CuO–CeO_2$ mixed oxide catalysts are very attractive for WGS reaction due to its high stabilities for use at high temperatures, the low cost of Cu and the fact that they do not require any in situ activation [2]. In addition, the $CuO–CeO_2$ catalysts, in contrast to commercial catalysts, which contain FeO in their formulations, are absolutely resistant to CO_2, H_2O and SO_2 thus avoiding deactivation during the WGS reaction [3,4]. Nevertheless, the catalytic activity of $CuO–CeO_2$ catalysts strongly depends on the interaction between the CuO and the CeO_2 [5–15]. Therefore, sol–gel Pechini method, in this context, is preferred technique, catalysts prepared show a high dispersion of CuO over CeO_2 particles [16].

However, the main problem of WGS reaction is that it produces a significant amount of CO_2, one of the most important greenhouse gases. Moreover, the presence of CO_2 as well as trace amount of unreacted CO in the anode stream lowers the performance of the fuel cells or even poison the electrode [17]. Thus, the H_2 must be purified for high purity applications and the CO_2 produced during the reaction must be captured and stored. Therefore, in this study, an alternative catalytic hollow fibre membrane micro-reactor (CHFMMR), which integrates both a catalytic micro-reactor and an H_2 selective membrane in the same unit, has been developed to produce a CO_x free H_2 by WGS reaction. The CHFMMR offers several advantages over existing H_2 production systems. First, the catalytic membrane micro-reactor works at significantly lower temperatures and/or using less amounts of catalyst compared to the conventional reactors. Furthermore, it combines the processes of generating and separating H_2 in a single step resulting in only H_2 being produced in the permeate stream of the reactor [18].

A successful CHFMMR should have a membrane with high H_2 permeability and selectivity combined with chemical, mechanical and thermal long-term stability. Pd membranes have been often employed for both H_2 purification [19] and catalytic membrane reactors [20–22], though they have drawbacks including hydrogen embrittlement and their moderate H_2 permeability at low temperatures. Recent efforts have been made in the development and optimization of the Pd alloy membranes such as the Pd/Ag membrane [23], which works in a greater temperature range and shows higher H_2 permeability than a Pd membrane.

Ceramic supports are usually employed in the development of conventional catalytic membrane reactors (CMRs), since the

* Corresponding author. Tel.: +44 0207 5945676; fax: +44 0207 5945629.
E-mail address: kang.li@imperial.ac.uk (K. Li).

0920-5861/$ – see front matter © 2011 Elsevier B.V. All rights reserved.
doi:10.1016/j.cattod.2011.03.083

combination of high chemical, thermal and mechanical resistance along with their small pores and narrow pore size distribution have made them an attractive alternative to polymeric and stainless steel supports. However, ceramic supports are currently produced as tubes with diameters of several millimetres, which have a low surface area/volume ratio. This is an important limitation in the development of CMRs, in which it is desirable to maximize the surface area/volume ratio of the membrane module in order to increase the permeation of the H_2 from the reaction zone.

The exceptional asymmetric pore structure of the Al_2O_3 hollow fibres [24], dense sponge-like structure in the outer border and open porous finger-like structure in the inner, make them an excellent support for both membrane and CuO/CeO_2 catalysts. A thin Pd or Pd/Ag layer can be deposited on the outer layer of the Al_2O_3 hollow fibre, because of its small pores and narrow pore size distribution. At the same time, the high geometric surface area of the finger-like region allows its deposition of CuO/CeO_2 catalysts. Moreover, the finger-like region can be viewed as one microreactor made up of hundreds of microchannels (dp = 10 μm) that are perpendicularly distributed around the lumen of the fibre. This novel catalyst distribution offers important advantages in comparison with the conventional packed bed catalyst distributions such as reduction of the pressure drop, increase of the catalytic surface to volume ratio and improvement of the heat and mass transfer and the mixing of gases during the reaction [25–29]. Finally, the modular and high surface area/volume ratio of the Al_2O_3 hollow fibres make them easily scale up by bundling the fibres in the unit [30].

In this study, a series of CuO/CeO_2 catalysts with a Cu content ranging from 5% to 40% have been synthesized by sol–gel Pechini method and tested in WGS reaction in a fixed-bed reactor. Based on the catalytic activity results, the most active catalyst was then deposited inside the finger-like region of the Al_2O_3 hollow fibre for the further development of both CHFMR and CHFMMR, the latter of which was fabricated by coating the Pd or Pd/Ag membrane on the outer layer of the Al_2O_3 hollow fibre using a single or multilayer electroless plating (ELP) technique. The performances of the CHFMR, Pd-CHFMMR and Pd/Ag-CHFMMR, were studied in details.

2. Experimental

2.1. Preparation of the CuO/CeO_2 catalysts

The CuO/CeO_2 catalysts were prepared using the sol–gel Pechini method. $Ce(NO_3)_3{\cdot}6H_2O$ (99.0% Fluka Analytical) and $Cu(NO_3)_2{\cdot}3H_2O$ (99% Acros Organic) were dissolved in 50 ml deionised water. The amount of $Ce(NO_3)_3{\cdot}6H_2O$ and $Cu(NO_3)_2{\cdot}3H_2O$ were varied to produce CuO/CeO_2 with different CuO loading. After both metal nitrates were fully dissolved, citric acid (99.0% Sigma–Aldrich) was added to the solution with a molar ratio of 2:1 between the citric acid and the metal ions. The process was continued by adding ethylene glycol into the solution and the molar ratio between citric acid and ethylene glycol was 1:1.2. The catalyst solutions were kept stirring for 3 h and later placed into an oven (Salvislab Thermocenter) for drying process at 115 °C for 24 h to form foamy dry gel. The dry gel was then calcined in a tubular furnace (Vecstar Furnaces, VCTF/SP) at 400 °C for an hour.

2.2. Characterization of the CuO/CeO_2 catalysts

X-ray diffraction measurements were performed with a Bruker AXS D8 ADVANCE diffractometer with $Co_{K\alpha 1}$ source ($\lambda = 0.178897$) in a wide angle range (from 30 to 90 in 2θ).

The specific surface area and the pore volume of the fresh catalysts were measured by N_2 adsorption isotherms at 77 K. An automatic TriStar 3000 volumetric system was used to obtain the gas adsorption isotherms. Prior to N_2 adsorption, the catalysts were degassed at 150 °C overnight. The BET model was used to obtain the specific surface area.

Temperature programmed reduction (TPR) was performed on a Micromeritics Autochem-II instrument equipped with a TCD detector. The samples (0.03 g) were prior dried in an Ar flow at 120 °C for 30 min. After the TCD signal was stable, the gas stream was switched to 50 ml/min 5% H_2/Ar (Linde). The temperature was raised from 25 to 900 at 10 °C/min.

2.3. Preparation of the Al_2O_3 hollow fibre

Asymmetric Al_2O_3 hollow fibre substrates, which have an OD = 1.9 mm and an ID = 1.0 mm, have been prepared using phase-inversion technique, followed by sintering at high temperatures. The detailed procedures in fabricating the substrates can be found elsewhere [24].

2.4. Preparation of the Pd and Pd/Ag membranes

The outer surface of the Al_2O_3 hollow fibre was coated with a thin and gas-tight layer of white glaze in order to block the pores of that area; only 10 cm in the central part of the Al_2O_3 hollow fibre was free where either the Pd or Pd/Ag membrane was deposited by electroless plating technique [31]. Prior to the activation process, the Al_2O_3 hollow fibres were cleaned using deionised water and activated subsequently by sequential dipping in $SnCl_2$–HCl (1 g/L, pH 2) and in $PdCl_2$–HCl (1 g/L, pH 2) solutions. The activation process was repeated six times, after which the surface colour of the Al_2O_3 hollow fibre changed from white to dark brown. The Al_2O_3 hollow fibres activated with Pd seeds were then coated with Pd and Pd/Ag using single or sequential multi-layer electroless plating technique, respectively. During the preparation of the Pd/Ag membrane, the Pd layer was deposited first and then the Ag layer, since the ability of Pd to penetrate into the pore support is higher than that of Ag [32]. Both Pd and Pd/Ag prepared membranes were dried in an oven at 120 °C for 2 h. Finally, a uniform Pd/Ag alloy was obtained by annealing to the Pd/Ag membrane in an H_2 atmosphere for 24 h at 400 °C.

2.5. Characterization of the Pd and Pd/Ag membranes

The morphology, structure and thickness of Pd and Pd/Ag membranes were studied using a scanning electron microscope (SEM, JEOL JSM-5610LV). Secondary electron (SE) and back-scattered electron (BSE) detectors were employed during the capture of the SEM images. Both top-surface and cross-section SEM images were recorded at different magnifications. Elemental analysis (line-scans) with an energy dispersive X-ray spectroscopy detector (EDS, INCA Energy by Oxford Instruments) was performed on the interphase between the Al_2O_3 hollow fibre support and the Pd/Ag membrane, before and after annealing in H_2 atmosphere at 400 °C for 24 h, in order to study the homogeneity of the final membrane. The samples were gold coated under vacuum for 3 min at 20 mA (EMITECH Model K550 LV) before SEM and EDS analysis.

Permeation tests using pure H_2 and Ar gases were carried out to study the permeability and selectivity of the prepared Pd and Pd/Ag membranes. The permeation measurements of both single gases through the membranes were studied in the temperature range between 300 °C and 450 °C and over the pressure range from 0.5 bar to 3.5 bar. The selectivity of the membrane ($S_{H_2/Ar}$) was defined as the ratio of the permeation flux of pure H_2 to pure Ar.

2.6. Deposition of 10% CuO/CeO_2 into the Al_2O_3 hollow fibre for development of both CHFMR and CHFMMR

Prior to the deposition of 10% CuO/CeO_2 catalyst into the fingers of the Al_2O_3 hollow fibre, the outer surface of both Al_2O_3 (in the case of CHFMR) and the Pd or Pd/Ag membrane (in the case of CHFMMR) was wrapped with the PTFE tape properly in order to prevent direct contact with the catalyst solution. A homogeneous catalyst solution was later injected into the lumen of the Al_2O_3 hollow fibre substrates using a glass pipette and this process was repeated several times. The Al_2O_3 hollow fibres were then dried in an oven (Salvislab Thermocenter) at 60 °C for 24 h and further dried at 115 °C to complete the polymerization of a polymeric resin precursor. The calcination process was later carried out by flowing 30 ml/min of air into the lumen-side of the Al_2O_3 hollow fibre at 400 °C for 1 h. In order to prevent the oxidation of the Pd or Pd/Ag membrane of the CHFMMR, 60 ml/min of Ar was flowed on the outer surface. The catalyst loading in the Al_2O_3 hollow fibre was obtained by measuring the weight of the Al_2O_3 hollow fibre substrates before and after calcination steps and was found to be around 8 mg in all cases. Finally, it is important to note, that in the development of the CHFMMR the deposition of 10% CuO/CeO_2 into the fingers of the Al_2O_3 hollow fibre was carried out after the fabrication of either Pd or Pd/Ag membranes in order to avoid the dissolution of copper into the plating solution due to the presence of ammonia and EDTA in the plating solution.

2.7. Catalytic activity

The catalytic activity measurements of the WGS reaction were tested in a fixed-bed reactor, a CHFMR and a CHFMMR operating under atmospheric pressure over a temperature range from 300 °C to 500 °C. The feed mixture in all cases contained Ar (90%), CO (5%) and H_2O vapour (5%) and was supplied to the reactor at a flow rate of 100 ml/min.

The catalytic activity tests in the fixed-bed reactor were carried out using 35 mg of catalysts. The catalyst with a particle size of approximately 100 μm, was mixed with 1.3 g of SiC and packed into a 6 mm ID ceramic tube. The packed-bed length was approximately 25 mm and the mass transfer limitation across the bed was negligible.

The catalytic activity tests in both CHFMR and CHFMMR were carried out in an open-both-end configuration, which enabled the reactants to flow through the lumen of the Al_2O_3 hollow fibre [33]. In a typical catalytic activity test the weight of the catalyst deposited inside the finger of the Al_2O_3 hollow fibre was 8 mg. A co-current sweep gas rate of 40 ml/min of Ar was used during the operation of the CHFMMR to create a concentration gradient across the Pd or Pd/Ag membrane. The H_2 recovery index, which represents the ability of the membrane to perform H_2 permeation is defined as follows:

$$H_2 \text{ recovery index}\,(\%) = \frac{F_{H_2}^{Permeate}}{F_{H_2}^{Permeate} + F_{H_2}^{Retentate}} \times 100 \quad (1)$$

The concentration of the products was measured using TCD gas chromatography (Varian-3900). The GC injections for gas analysis for every reactor used in this study were repeated three times to obtain more reliable results. The CO conversion is defined as follows:

$$\text{CO conversion}\,(\%) = \frac{1 - F_{CO}^{out}}{F_{CO}^{in}} \times 100 \quad (2)$$

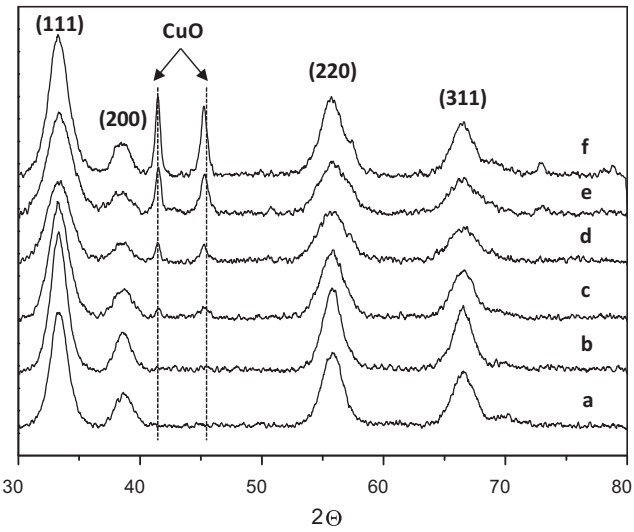

Fig. 1. XRD patterns of CuO/CeO_2 catalysts: (a) 5% CuO/CeO_2, (b) 7.5% CuO/CeO_2, (c) 10% CuO/CeO_2, (d) 20% CuO/CeO_2, (e) 30% CuO/CeO_2 and (f) 40% CuO/CeO_2.

3. Results and discussion

The XRD patterns of CeO_2 and fresh CuO/CeO_2 catalysts, prepared by the sol–gel Pechini method, are shown in Fig. 1a–f. All the samples presented show characteristic cubic fluorite CeO_2 reflection peaks. However, the monoclinic CuO reflection peaks were only observed in catalysts with Cu loadings higher than 7.5%, which progressively increased in intensity with the Cu loadings. There were no observed reflection peaks that could be associated with a metallic Cu phase in any of the catalysts.

The fact that at Cu loadings lower than 7.5% the CuO could not be detected by XRD analysis can be attributed to one of the following phenomena: the CuO particles are highly dispersed on the CeO_2 and consequently they are too small (dp < 2 nm) [34] or the Cu is interacting with the CeO_2 forming a solid solution Cu–Ce–O [35]. It is quite accepted according to the literature that non-crystalline CuO could be explained by a combination of both above phenomena, occurring at the same time. In this respect, it was also observed that according to the quantitative phase analysis about 27 wt% of the Cu, in 30% CuO/CeO_2 and 20% CuO/CeO_2 catalysts, is not detected by XRD analysis. These results indicate that both crystalline and non-crystalline CuO coexists in these catalysts. Similar results have been reported for CuO/CeO_2 catalysts with higher Cu loadings [36–40].

The CeO_2 and the CuO crystallite particle sizes were determined from the XRD results by Scherrer analysis of the peaks (1 1 1) at 33.4° and (1 1 1) at 45.5°, respectively as shown in Table 1. Although in Fig. 1d some of the monoclinic CuO reflection peaks can be recognized, it was not possible to calculate a reliable value for the CuO crystallite particle size due to the signal to noise ratio and the low intensity of these reflection peaks. Table 1 shows that the

Table 1
Physical properties of CuO/CeO_2 catalysts synthesized by sol–gel Pechini method.

Samples	S_{BET} (m^2/g)	Pore volume (cm^3/g)	Crystallite size (nm)	
			CeO_2	CuO
CeO_2	27	0.081	5.4	–
5%CuO/CeO_2	30	0.074	5.3	–
7.5%CuO/CeO_2	50	0.037	5.5	–
10%CuO/CeO_2	112	0.142	4.6	–
20%CuO/CeO_2	122	0.124	3.7	9.4
30%CuO/CeO_2	79	0.100	4.3	14.0
40%CuO/CeO_2	58	0.070	4.5	17.3

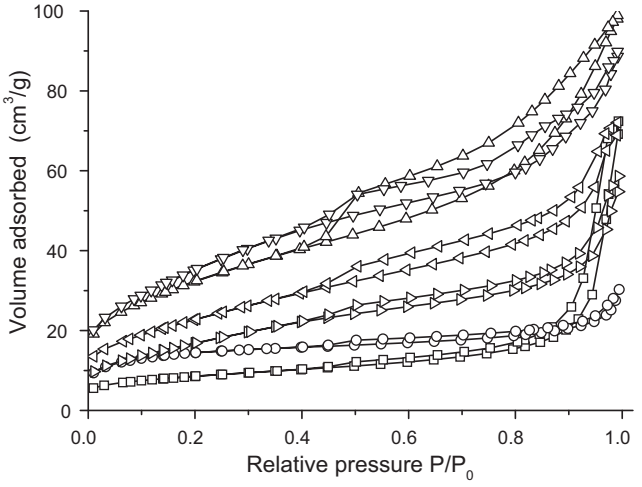

Fig. 2. Adsorption isotherm of N_2 at −198 °C: (□) 5% CuO/CeO_2, (○) 7.5% CuO/CeO_2, (△) 10% CuO/CeO_2, (▽) 20% CuO/CeO_2, (◁) 30% CuO/CeO_2 and (△) 40% CuO/CeO_2.

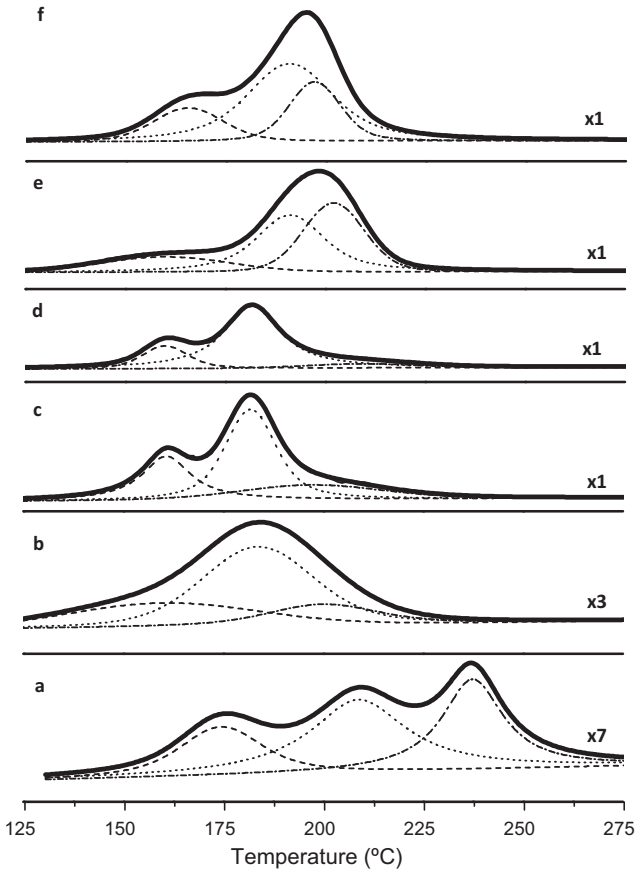

Fig. 3. H_2-TPR profiles of CuO/CeO_2 catalysts: (a) 5% CuO/CeO_2, (b) 7.5% CuO/CeO_2, (c) 10% CuO/CeO_2, (d) 20% CuO/CeO_2, (e) 30% CuO/CeO_2 and (f) 40% CuO/CeO_2.

CeO_2 crystallite particle size decreased with the Cu loadings reaching its minimum value at 20%, i.e. the CeO_2 crystallite particle size in 20% CuO/CeO_2 is about 30% smaller than in the pure CeO_2. This behaviour suggests that the non-crystalline CuO acts to increase the thermal stability of the CeO_2 particles avoiding crystal growth during the calcination step [41–43]. Nevertheless, the CeO_2 crystallite particle size increases again for Cu loadings higher than 20%. This behaviour seems to be related with the fact that large CuO crystallite particle sizes ($dp \geq 13$ nm) have been observed for these Cu loadings, which indicates the low concentration of non-crystalline CuO in these catalysts and consequently the lower thermal stability of the CeO_2 particles.

The N_2 adsorption–desorption isotherms at 77 K corresponding to the CuO/CeO_2 catalysts are shown in Fig. 2. All the catalysts show a type IV N_2 adsorption–desorption isotherm, according to the Brunauer–Deming–Deming–Teller (BDDT) classification [44], which is typical of mesoporous materials. The hysteresis loop could be ascribed to either type H3 or type A, according to the IUPAC or De Boer classifications, respectively [45]. This hysteresis loop confirms the presence of mesopores and it is typically reported for materials having pores with slit-like shapes.

Specific surface areas calculated by application of the BET method to the N_2 adsorption–desorption isotherms at −198 °C are summarized in Table 1. A gradual increase of the specific surface area values as the Cu content increases was observed from 5% to 20% Cu loadings. However, the specific surface area values decreased for Cu loadings higher than 20%. Although, in some cases it has been reported that the specific surface area seems to be independent of the Cu content and it is primarily influenced by CeO_2 particle morphology [46], in this study, the changes in the specific surface area values could be tentatively related with the Cu content as explained below.

The uniform distribution of the Cu and Ce cations on the organic gel obtained after etherification and polymerization steps by using the sol–gel Pechini method, allows not only a high dispersion of the CuO on the catalyst but also the avoidance of the sintering of the CeO_2 particles during the calcination step. Based upon this, the addition of CuO that acts as a structural promoter significantly enhances the specific surface area of the CuO/CeO_2 system by thermal stabilization of the CeO_2 particles. Nevertheless, the smaller specific surface area of both 30% CuO/CeO_2 and 40% CuO/CeO_2 catalysts along with a 56% decrease in the pore volume observed from 20% to 40% Cu loadings suggest that the increase in the proportion of large CuO particles ($14\text{ nm} < dp < 17.3\text{ nm}$), when Cu loading is higher than 20%, blocks the CeO_2 porosity decreasing the specific surface area.

The deconvolution H_2-TPR profiles of CuO/CeO_2 catalysts are shown in Fig. 3. It was observed that the feature of each H_2-TPR profile was highly dependent on the Cu contained, showing that more than one CuO species coexists in all the catalytic systems studied. It is well known that CeO_2 has two reduction peaks at 400 °C and at 900 °C, which are ascribed to the reduction of surface and bulk oxygen, respectively. Meanwhile, CuO only has a single reduction peak at about 280 °C. When CuO is incorporated to the CeO, the redox properties of the CuO/CeO_2 system is greatly promoted due to the interaction occurring at the interface between CuO and the surface oxygen vacancies of CeO_2, shifting the reduction peaks to below or around 200 °C. According to the literature, the H_2-TPR profiles have been deconvoluted in the following three components: small highly dispersed CuO strongly interacting with the CeO_2 particles (125–175 °C) [47,48], large CuO particles on the CeO_2 surface particles (175–200 °C) [49,40] and large CuO particles unassociated with CeO_2 particles (200–250 °C) [50,51]. The reduction temperature, shape and intensity of each component provide useful information for an overview of the surface composition of each catalytic system.

The first contribution, due to small highly dispersed CuO particles on the CeO_2 surface, can be observed in all the catalysts; the reduction temperature decreased with increasing the Cu content up to 20% and then increased again. This behaviour indicated that 20% CuO/CeO_2 catalyst showed the strongest synergistic interaction between the CuO particles and CeO_2 surface. Moreover, a significant contribution due to the formation of CuO particles ($dp \leq 10$ nm) on the CeO_2 surface was observed for catalysts with a Cu content from 7.5% to 20%. However, it was irrelevant for Cu content higher than

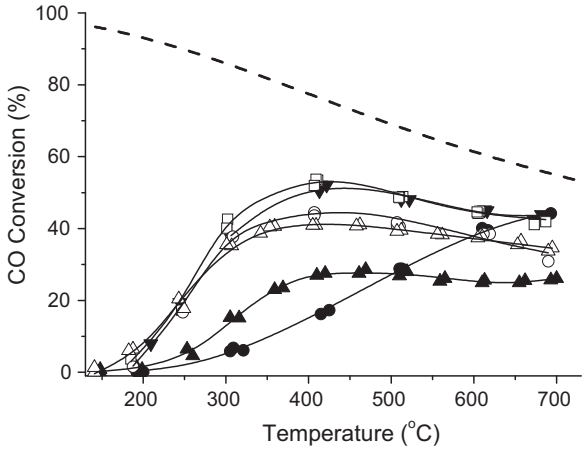

Fig. 4. CO conversion as a function of the temperature in WGS reaction using a fixed-bed reactor: (---) thermodynamic equilibrium, (●) 5% CuO/CeO_2, (▲) 7.5% CuO/CeO_2, (□) 10% CuO/CeO_2, (▼) 20% CuO/CeO_2, (○) 30% CuO/CeO_2 and (△) 40% CuO/CeO_2.

20%, where the most important contribution was due to larger CuO particles (10 nm > dp > 17 nm) unassociated with CeO_2 particles.

The catalytic activity of CuO/CeO_2 samples in the WGS reaction is shown in Fig. 4. The reaction conditions were fixed in order to test all the catalysts under the thermodynamic equilibrium line, to facilitate the comparison between each catalyst.

In all cases with the exception of 5% CuO/CeO_2 catalyst, the CO conversion increased with an increase in temperature to 400 °C and then it either steadily decreased or remained constant. This behaviour suggests that the high dispersion of the Cu nanoparticles in a 5% CuO/CeO_2 catalyst is too small to be detected by XRD (dp < 2 nm), prevented their sintering at high temperature avoiding their deactivation. Hence, the high thermal stability of the 5% CuO/CeO_2 catalyst makes it an excellent option for WGS reaction at high temperatures.

On the other hand, Fig. 4 also shows that the catalytic activity increased with the increase of the Cu loading and reached a maximum CO conversion of 52% at 400 °C when the Cu loading was between 10% and 20%, then the catalytic activity decreased with the Cu loading. This behaviour indicates that the Cu loading is a main factor for catalytic activity. However, at low temperatures, from 150 °C to 300 °C, the CO conversion was the same for the catalysts with a Cu loading higher than 7.5%.

On the other hand, it is important to note the correlation that exists between the specific surface area of the catalysts and their catalytic activity as shown in Table 1. The fact that the higher the surface area, the higher the catalytic activity is, suggests that the highly porous nano-crystalline CeO_2 morphology in 10% CuO/CeO_2 and 20% CuO/CeO_2 catalysts is probably one of the reasons for their high CO conversion in the WGS reaction. Moreover, the catalytic activity results also indicate that the highly dispersed small CuO particles strongly interacting with the CeO_2 particles, observed during the H_2-TPR experiments, showed the highest catalytic activity. As is well known, the synergistic interaction between the CuO particles and CeO_2 surface along with the Cu particle size and the number of oxygen vacancies of the CeO_2 plays an essential role for a high catalytic activity in WGS reaction.

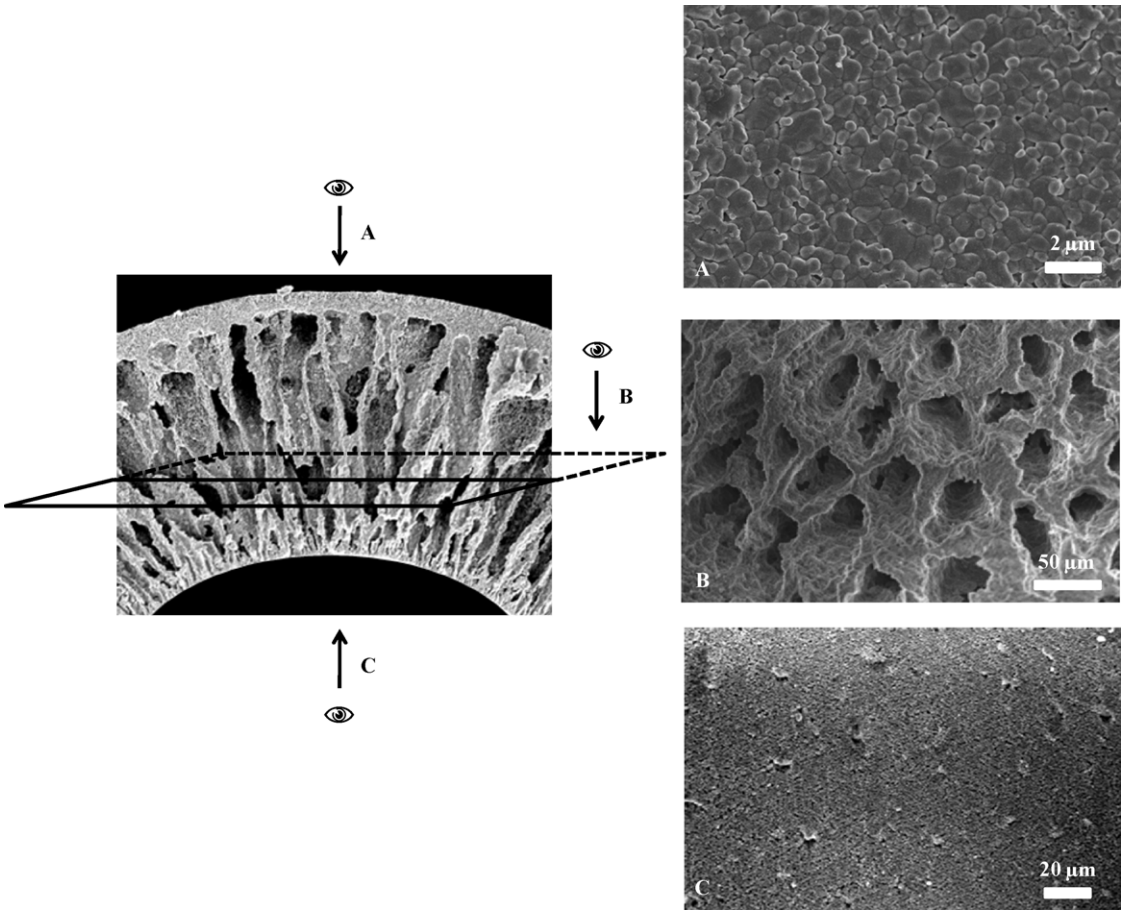

Fig. 5. SEM picture of the cross-section of a typical Al_2O_3 hollow fibre employed in this work. (A) Top view of the outer layer surface, (B) horizontal cross section of the shell and (C) inner surface.

Based on these results, a 10% CuO/CeO_2 catalyst, which showed the highest catalytic activity in a WGS reaction was deposited inside the finger-like region of the Al_2O_3 hollow fibre in the development of both catalytic hollow fibre micro-reactor (CHFMR) and catalytic hollow fibre membrane micro-reactor (CHFMMR). Two different membranes were tested in the CHFMMR: Pd and Pd/Ag membranes.

Fig. 5 shows a different SEM picture of a typical Al_2O_3 hollow fibre employed in this work as a support of both catalyst and Pd or Pd/Ag membrane. An asymmetric pore structure can be clearly observed, which consists of finger-like and sponge-like regions occupying approximately 80% and 20% of the fibre cross-section, respectively. The different pore sizes between the finger-like (dp = 10 μm) and the sponge-like (dp = 0.1 μm) regions given by Kingsbury and Li [24] allows the deposit of the catalysts into the finger-like region at the same time coating the outer layer of the Al_2O_3 hollow fibre with a thin Pd or Pd/Ag membrane.

Fig. 6A and B shows the SEM pictures of the cross section of the Al_2O_3 hollow fibre after Pd and Pd/Ag membrane deposition. A back-scattered electron detector was employed during the capture of both photos, in order to increase the contrast between both phases: Al_2O_3 hollow fibre support and Pd or Pd/Ag membrane. It can be observed that the deposition of both Pd and Pd/Ag membranes was uniform all around the outer layer of the Al_2O_3 hollow fibre with a total thickness of about 5 μm for Pd/Ag as confirmed in Fig. 7.

The elemental composition along the cross-section of the Pd/Ag membrane (see the arrow in Fig. 6B) was determined using EDX. Fig. 7a and b shows the EDX line scans of the Pd/Ag membrane cross-section before and after annealing at 400 °C for 24 h in an H_2 atmosphere, respectively. In both cases two different zones can be clearly observed: (I) the Al_2O_3 support and (II) the Pd/Ag layer. Although Fig. 7a shows that the composition profile along the Pd/Ag membrane was non-uniform, Fig. 7b shows a very uniform distribution of Pd and Ag along the membrane. This behaviour suggests firstly, that the deposition of the Pd layer was not uniform and did not fully cover the Al_2O_3 surface and as a result Ag can be observed on the surface of the Al_2O_3 hollow fibre. Secondly, a uniform Pd/Ag alloy was produced during annealing. Finally, intermetallic diffusion between the Al_2O_3 hollow fibre support and the Pd/Ag membrane was not observed, even though during the annealing process the membrane was heated at a high temperature (400 °C) for a long time (24 h).

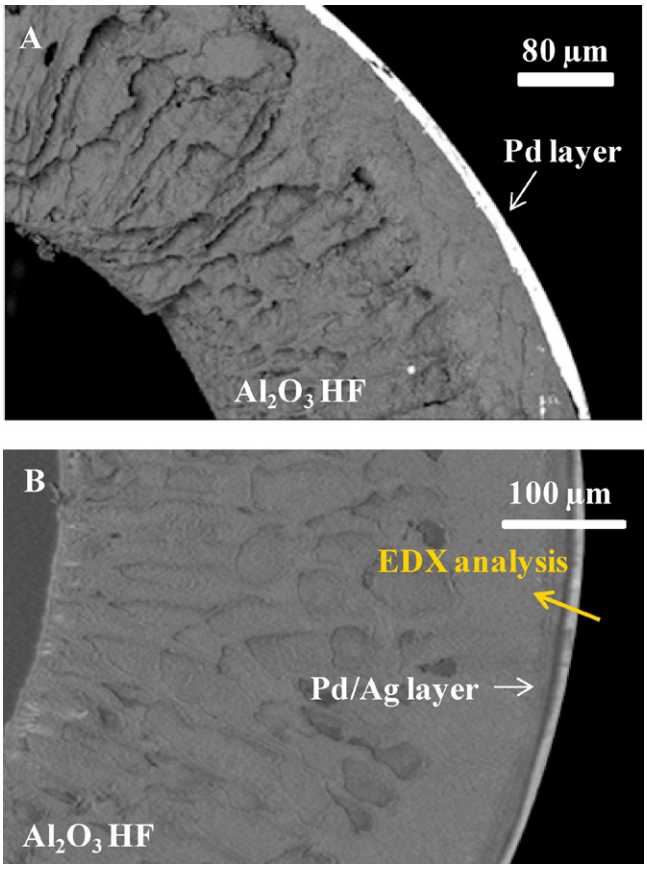

Fig. 6. SEM pictures of the cross-section of the Al_2O_3 hollow fibre after (A) Pd membrane deposition and (B) Pd/Ag membrane deposition.

Permeation tests were carried out on the Pd and the annealed Pd/Ag membranes using pure H_2 and Ar gases in order to test the H_2 permeability and H_2/Ar selectivity before being tested in the CHFMMR. Fig. 8a and b shows both H_2 and Ar permeation fluxes

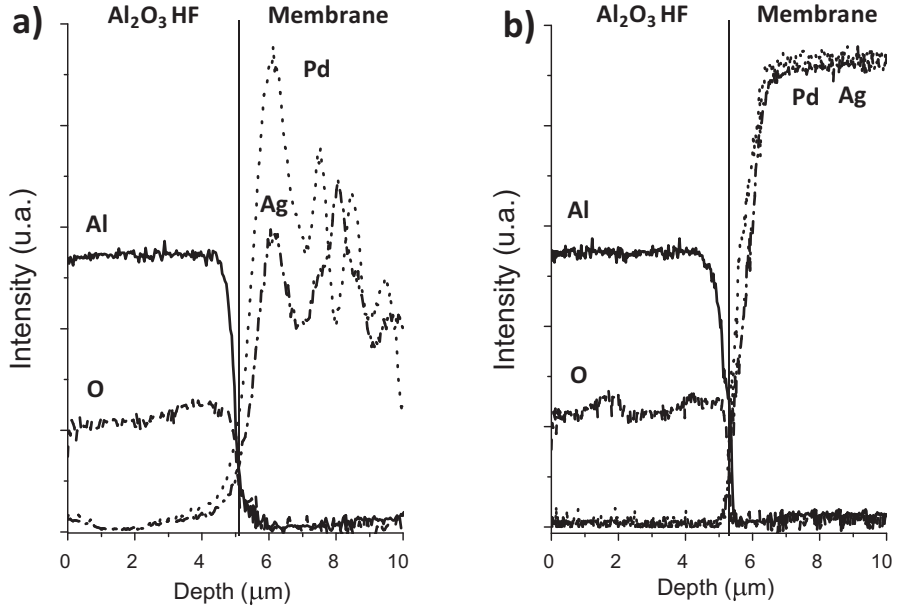

Fig. 7. EDX line scans of: Pd/Ag membrane cross-section (a) before and (b) after annealing at 400 °C for 24 h in H_2 atmosphere.

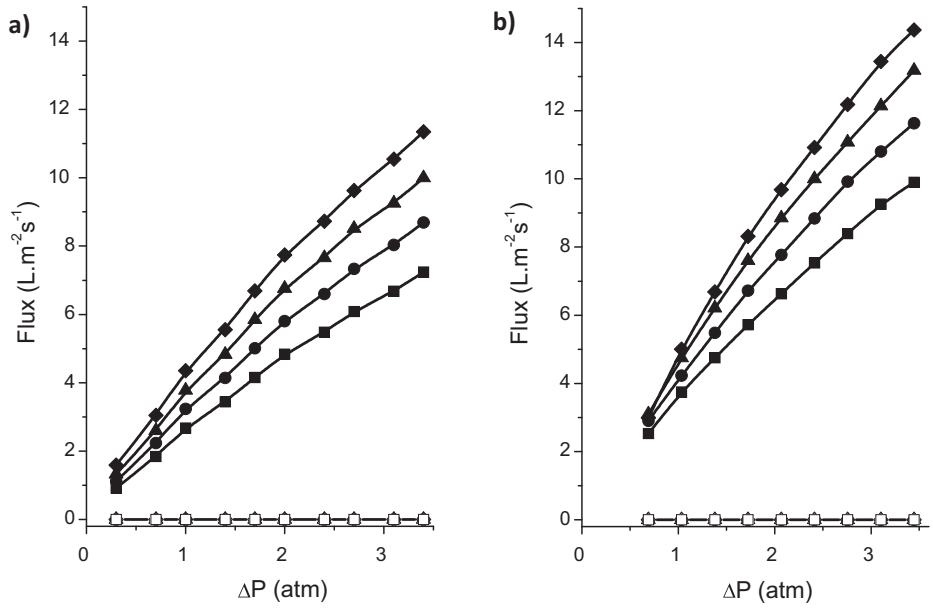

Fig. 8. Fluxes of pure gases through the (a) Pd membrane and (b) Pd/Ag membrane as a function of the difference of the transmembrane pressure at different temperatures: 300 °C (■) H_2 and (□) Ar, 350 °C (●) H_2 and (○) Ar, 400 °C (▲) H_2 and (△) Ar and 450 °C (♦) H_2 and (◊) Ar.

through the Pd and the annealed Pd/Ag membranes, respectively, as a function of the pressure difference calculated between shell and lumen sides. It can be observed that for both membranes the H_2 permeation increased as the temperature and/or the pressure in the lumen of Al_2O_3 hollow fibre was increased. The permeation data given in Table 2 shows that the H_2 permeances of the Pd/Ag membrane were about 25% higher than that of the Pd membrane, although the Ag concentration on the membrane was 50%, which is not the optimum 23% [52]. On the other hand, Ar did not permeate through both the Pd and the annealing Pd/Ag membranes at any testing conditions applied during the permeation tests, showing an infinite selectivity towards H_2. Based on these results, it can be concluded that both the Pd and Pd/Ag membranes coated on the Al_2O_3 hollow fibre was absolutely dense and free from defects.

Fig. 9a shows the CO conversion in WGS reaction at different temperatures using a fixed-bed reactor, CHFMR, Pd-CHFMMR and Pd/Ag-CHFMMR. It is important to note that the amount of catalyst deposited inside the finger-like region of the Al_2O_3 hollow fibre was 8 mg, which was three times smaller than those tested in the fixed bed reactor (see Fig. 4), as the small volume of the finger-like

Table 2
H_2 permeability and H_2/Ar selectivity of both Pd and Pd/Ag membranes.

Temperature (°C)	Pd membrane		Pd/Ag membrane (after annealing)	
	H_2 permeances ($L\,m^{-2}\,s^{-1}\,atm^{-1/2}$)	$S_{H_2/Ar}$	H_2 permeances ($L\,m^{-2}\,s^{-1}\,atm^{-1/2}$)	$S_{H_2/Ar}$
300	6.9	∞	9.1	∞
350	8.3	∞	10.8	∞
400	9.5	∞	12.4	∞
450	10.7	∞	14.1	∞

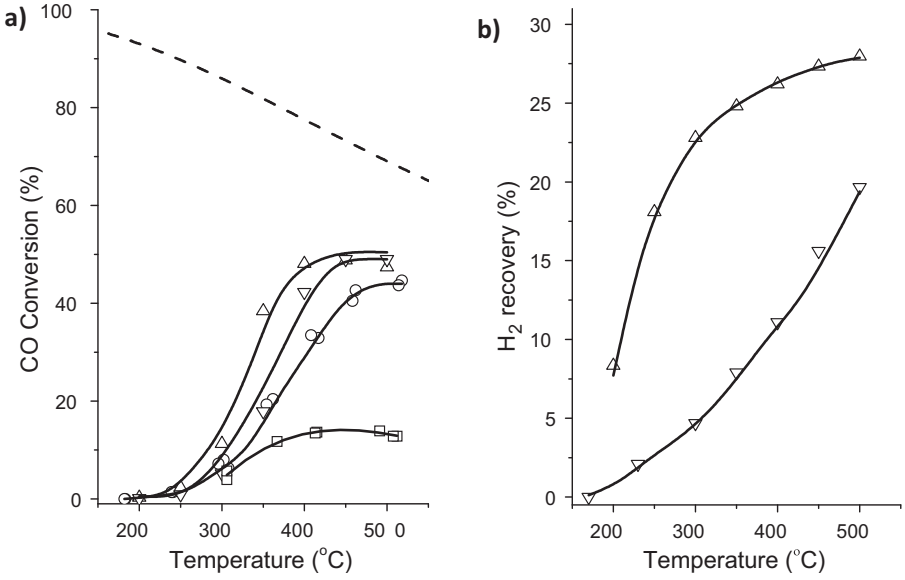

Fig. 9. (a) CO conversion as a function of the temperature in WGS reaction: (---) thermodynamic equilibrium, (□) fixed-bed reactor, (○) CHFMR, (▽) Pd-CHFMMR, (△) Pd/Ag-CHFMMR. (b) H_2 recovery during WGS reaction as a function of the temperature using (▽) a Pd membrane and (△) a Pd/Ag membrane.

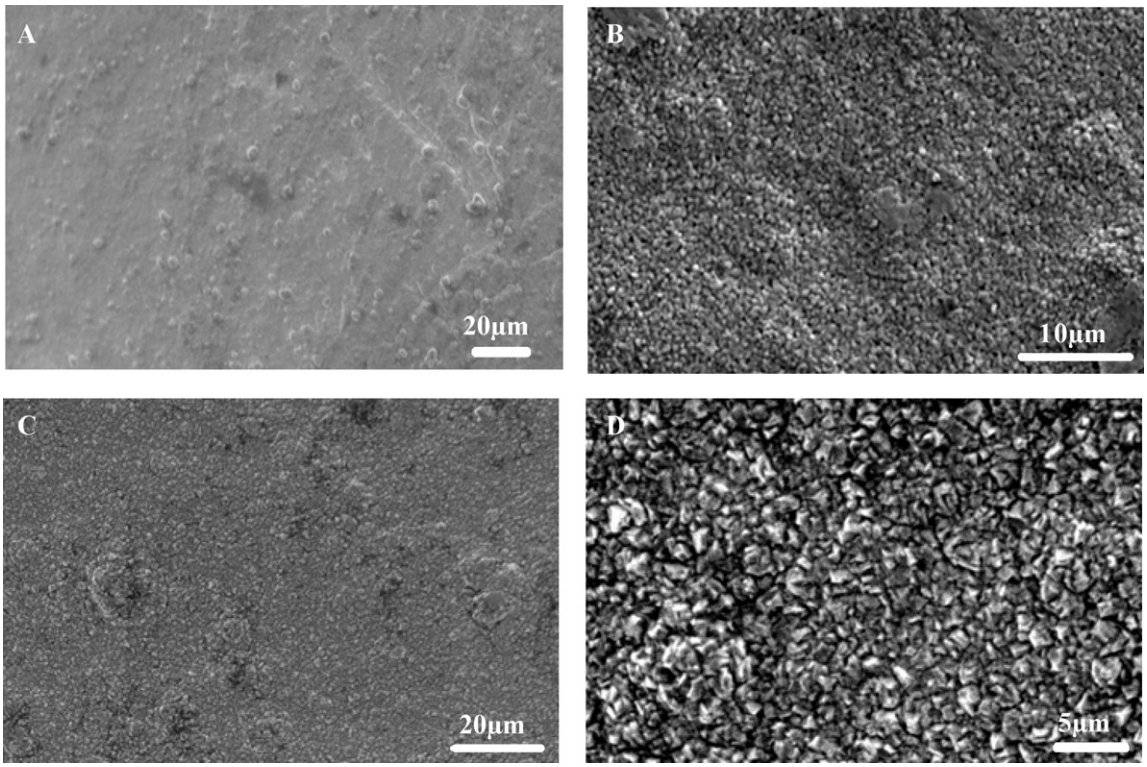

Fig. 10. SEM pictures at different magnifications of the top surface of (A and B) the Pd membrane and (C and D) the Pd/Ag membrane.

region of the Al_2O_3 hollow fibres prevented further deposition of the catalyst. Fig. 9a shows that under similar reaction conditions the CO conversion obtained in the CHFMR is significantly larger than that obtained in a fixed-bed reactor. This improvement in the CO conversion, a 30% increase at 450 °C, can be explained by the use of Al_2O_3 hollow fibres as a substrate resulting in a more efficient utilization of the catalyst compared to conventional fixed-bed configurations. As we have reported in our previous work [53], the dispersion of the catalyst inside the finger-like microchannels of the Al_2O_3 hollow fibres improves the catalytic surface to volume ratio, the heat and mass transfer as well as the mixing of gases during the reaction.

In order to improve the CO conversion, a Pd-CHFMMR, which integrates both a CHFMR and a Pd membrane in the same unit was developed and tested in WGS reaction. The Pd-CHFMMR offers several advantages over the CHFMR and the fixed-bed reactor. First, Pd-CHFMMR combines, in a single step, the processes of generating and separating H_2, due to high selectivity of the Pd, resulting in that only H_2 is produced as the reaction takes place in the reactor. Secondly, it can be observed in Fig. 9a that Pd-CHFMMR works at significantly lower temperatures than the CHFMR and the fixed-bed reactor. This behaviour can be explained by the fact that, in accordance with the "Le Chatelier" principle, the removal of one or more reaction products will shift the conversion towards product formation. Hence, an increase in the CO conversion to 10% and 35% from the corresponding values of the CHFMR and fixed bed reactor, respectively, was observed by using the Pd-CHFMMR.

A thin Pd/Ag alloy membrane was used in the Pd/Ag-CHFMMR in order to increase the H_2 recovery during the WGS reaction, because of its high H_2 permeances in comparison with a pure Pd membrane. Fig. 9a shows that the CO conversion in the Pd/Ag-CHFMMR was significantly improved with respect to Pd-CHFMMR; i.e. at 350 °C the CO conversion in the Pd/Ag-CHFMMR was double that obtained in the Pd-CHFMMR. Moreover, it is important to highlight that the high H_2 permeances of the Pd/Ag alloy membrane allows its operation at lower temperatures than a Pd membrane. As is shown in Fig. 9a, the effects of the Pd/Ag alloy membrane in the CO conversion become visible at 250 °C whereas for the Pd membrane it was not visible up to 300 °C. This behaviour suggests that the Pd/Ag alloy membrane could be a very promising candidate for WGS reaction at low temperature. However, although the CO conversion was significantly enhanced by using the Pd/Ag-CHFMMR (a 37% increase at 450 °C), it was not possible to reach and exceed the thermodynamic equilibrium line. This result is a consequence of the small amount of catalysts deposited into the finger-like microchannels of the Al_2O_3 hollow fibres. Nevertheless, since the Al_2O_3 hollow fibres have a tubular geometry with an outer diameter smaller than 2 mm, it is relatively easy to scale up by bundling the Al_2O_3 hollow fibres to a module, which makes it possible to pass the thermodynamic equilibrium line if additional fibres are used.

In order to compare the performance of both Pd and Pd/Ag membranes during the operation of the CHFMMR, the H_2 recovery index was calculated at different temperatures, as shown in Fig. 9b. This index is typically used to describe the efficiency of the membranes and can be defined as the H_2 fraction permeated through the membrane with respect to the total amount of H_2 produced during the WGS reaction. As can be seen, in both Pd and Pd/Ag membranes, the H_2 recovery index increased as the temperature was increased from 200 °C to 500 °C. Nevertheless, for the Pd membrane the H_2 recovery index increased almost linearly; whereas, for the Pd/Ag membrane it increased exponentially. Moreover, the H_2 index recovery was significantly higher for the Pd/Ag membrane than that of the Pd membrane, especially in the temperature range from 250 °C to 400 °C. This behaviour suggests that the different solubility and diffusion of the H_2 in Pd and Pd/Ag alloy systems [54,55]. On the other hand, the low H_2 index recovery observed even at high temperatures, i.e. 19% and 27% at 500 °C for Pd and Pd/Ag, respectively, suggests that the pressure difference across

both membranes produced by using 40 ml/min of Ar as a sweep gas was very low.

Finally, both Pd and Pd/Ag membranes deposited on the outer layer of the Al_2O_3 hollow fibre in the CHFMMR showed an excellent stability during the WGS reaction, even though they were tested at higher temperatures (500 °C) for long periods of time (24 h). Fig. 10A–D shows the top surface of both Pd and the Pd/Ag membranes after WGS reaction at different magnifications. Based on these SEM photos, we can conclude that both membranes were fully dense and free of defects after the WGS reaction.

4. Conclusions

In this study, CuO/CeO_2 catalysts with a Cu content range from 5% to 40% have been synthesized by the sol–gel Pechini method and tested in a WGS reaction in a fixed-bed reactor. According to XRD results, the high dispersion of the CuO nanoparticles on CuO/CeO_2 catalysts prevented the sintering of the CeO_2 particles at high temperature avoiding catalytic deactivation during the WGS reaction. Moreover, it was observed that the catalytic activity increased with the specific surface area, which suggests that the highly porous nano-crystalline CeO_2 particle morphology is probably one of the main reasons for the high catalytic activity in the WGS reaction. According to these results, 10% CuO/CeO_2 catalyst which showed the highest catalytic activity in the WGS reaction was successfully deposited inside the finger-like region of the Al_2O_3 hollow fibre by the sol–gel Pechini method in the development of both CHFMR and CHFMMR.

Fully dense and uniform Pd and Pd/Ag membranes with a total thickness of about 5.0 μm were deposited on the outer layer of the Al_2O_3 hollow fibre by electroless plating technique before catalyst deposition. A uniform Pd/Ag alloy across the membrane was produced after annealing the Pd/Ag membrane in a H_2 atmosphere for 24 h at 400 °C. The H_2 permeances of the annealed Pd/Ag membrane was about 25% higher than that of the Pd membrane, even though the Ag concentration on the membrane was 50%, which is not the optimum concentration of 23%. An infinite H_2 selectivity through both Pd and Pd/Ag membranes was observed in the temperature and pressure ranges studied.

The CO conversion obtained in the WGS reaction using the CHFMR was three times larger than that in a conventional fixed-bed reactor, due to the deposition of the 10% CuO/CeO_2 catalyst into the finger-like region of the Al_2O_3 hollow fibres resulting in a more efficient utilization of the catalyst. In addition, the presence of both Pd and Pd/Ag membranes in the CHFMMR increased in a 10% and 20% CO conversion at 350 °C, respectively. Both Pd and Pd/Ag membranes deposited on the outer layer of the Al_2O_3 hollow fibre in the CHFMMR showed an excellent stability during the WGS reaction, even though they were tested at higher temperatures (500 °C) for long periods of time (24 h).

Based upon these results, the Pd/Ag-CHFMMR offers exclusive advantages over existing H_2 production systems and can be presented as an extremely promising system to produce CO_x-free H_2 by WGS reaction. Furthermore, the fabrication techniques and understanding of the process generated from this study are generic and may be applied to a wide range of heterogeneously catalysed gas phase reactions related to H_2 production.

Acknowledgment

The authors gratefully acknowledge the research funding provided by EPSRC in the United Kingdom (grant No. EP/G01244X/1).

References

[1] D.S. Newsome, Catal. Rev. Sci. Eng. 21 (1980) 275.
[2] L. Li, Y. Zhan, Q. Zheng, Y. Zheng, C. Chen, Y. She, X. Lin, K. Wei, Catal. Lett. 130 (2009) 532.
[3] W. Liu, A.F. Sarofim, M. Flytzani-Stephanopoulos, Appl. Catal. B 4 (1994) 167.
[4] C.R.F. Lund, Final Report to the U.S. Department of Energy, Grant DE-FG26-99FT40590, August 2002.
[5] F. Zhou, X.M. Zhao, H. Xu, C.G. Yuan, J. Phys. Chem. C 111 (2007) 1651.
[6] H.M. Yang, C.H. Huang, A.D. Tang, X.C. Zhangm, W.G. Yang, Mater. Res. Bull. 40 (2005) 1690.
[7] F. Bondioli, A. Bonamartini Corradi, C. Leonelli, T. Manfredini, Mater. Res. Bull. 34 (1999) 2159.
[8] D. Barreca, A. Gasparotto, C. Maccato, C. Maragno, E. Tondello, Langmuir 22 (2006) 8639.
[9] D.S. Zhang, H.X. Fu, L.Y. Shi, C.S. Pan, Q. Li, Y.L. Chu, W.J. Yu, Inorg. Chem. 46 (2007) 2446.
[10] B. Gu, Z.H. Wang, D.M. Han, C. Shi, G.S. Guo, Mater. Sci. Eng. B 139 (2007) 62.
[11] F.H. Scholes, A.E. Hughes, S.G. Hardin, P. Lynch, P.R. Miller, Chem. Mater. 19 (2007) 2321.
[12] H.Y. Chang, H.I. Chen, J. Cryst. Growth 283 (2005) 457.
[13] K.B. Zhou, Z.Q. Yang, S. Yang, Chem. Mater. 19 (2007) 1215.
[14] L.D. Mai, Y.W. Sun, R. Zhang, W. Si, H.P. Feng, H.C. Zhang, C.H. Liu, J. Yan, Phys. Chem. B 109 (2005) 24380.
[15] C. Laberty-Robert, J.W. Long, E.M. Lucas, K.A. Pettigrew, R.M. Stroud, M.S. Doescher, D.R. Rolison, Chem. Mater. 18 (2006) 50.
[16] M. Kakihana, J. Sol–Gel Sci. Technol. 6 (1996) 55.
[17] N. Rajalakshm, T.T. Jayanth, K.S. Dhathathreyan, Fuel Cell 3 (2003) 177.
[18] Catalysis in membrane reactors, Catal. Today 104 (2005) 101.
[19] G.Q. Lu, J.C. Diniz da Costa, M. Duke, S. Giessler, R. Socolow, R.H. Williams, T. Kreutz, J. Colloid Interface Sci. 314 (2007) 589.
[20] F.R. Garcia-Garcia, Y.H. Ma, I. Rodriguez-Ramos, A. Guerrero-Ruiz, Catal. Commun. 9 (2008) 482.
[21] J.N. Armor, Catal. Today 25 (1995) 199.
[22] P. Ferreira-Aparici, I. Rodriguez-Ramos, A. Guerrero-Rui, Appl. Catal. A: Gen. 237 (2002) 239.
[23] Y.H. Ma, B.C. Akis, M.E. Ayturk, F. Guazzone, E.E. Engwall, I.P. Mardilovich, Ind. Eng. Chem. Res. 43 (2004) 2936.
[24] B.F.K. Kingsbury, K. Li, J. Membr. Sci. 328 (2009) 134.
[25] Y. Han, N. Shikazono, Int. J. Multiphase Flow 35 (2009) 896.
[26] N. Dupont, G. Germani, A.C. van Veen, Y. Schuurman, G. Schafer, C. Mirodatos, Int. J. Hydrogen Energy 32 (2007) 1443.
[27] S. Tadepalli, R. Halder, A. Lawal, Chem. Eng. Sci. 10 (2007) 2663.
[28] H. Nagasawa, K. Mae, Ind. Eng. Chem. Res. 45 (2006) 2179.
[29] K. Sreenath, S. Pushpavanam, Chem. Eng. J. 155 (2009) 312.
[30] Y. Kikutani, A. Hibara, K. Uchiyama, H. Hisamoto, M. Tokeshi, T. Kitamori, Lab Chip 2 (2002) 193.
[31] P.P. Mardilovich, Y. She, Y.H. Ma, M.H. Rei, AIChE J. 44 (1998) 310.
[32] J.N. Keuler, L. Lorenzen, R.D. Sanderson, V. Prozesky, W.J. Przybylowicz, Thin Solid Films 347 (1999) 91.
[33] M.A. Rahman, F.R. Garcia-Garcia, M.D. Irfan Hatim, B.F.K. Kingsbury, K. Li, Appl. Catal. A 393 (2011) 71.
[34] P. Djinovic, J. Batista, B. Cehic, P. Albin, J. Phys. Chem. A 114 (2010) 3939.
[35] G. Avgouropoulos, T. Ioannides, Appl. Catal. A 244 (2003) 155.
[36] Y. Li, Q. Fu, M. Flytzani-Stephanopoulos, Appl. Catal. B: Environ. 27 (2000) 179.
[37] C. Zerva, C.J. Philippopoulos, Appl. Catal. B: Environ. 67 (2006) 105.
[38] P. Djinović, J. Batista, A. Pintar, Appl. Catal. A: Gen. 347 (2008) 23.
[39] D.H. Kim, J.E. Cha, Catal. Lett. 86 (2003) 107.
[40] W. Liu, M. Flytzani-Stephanopoulos, Chem. Eng. J. 64 (1996) 283.
[41] J.B. Dow, T.J. Huang, J. Catal. 100 (1996) 171.
[42] Q. Fu, W. Adam, M. Flytzani-Stephanopoulos, Catal. Lett. 77 (2001) 87.
[43] T. Xiaolan, Z. Baocai, L. Yong, X. Yide, X. Qin, S. Wenjie, Catal. Today 93 (2004) 191.
[44] S. Brunauer, L.S. Deming, W.E. Deming, E. Teller, J. Am. Chem. Soc. 62 (1940) 1723.
[45] G.D. Parfitt, K.S.W. Sing, Characterization of Powder Surfaces, vol. 44, Academic Press, 1976.
[46] B. Skårman, T. Nakayama, D. Grandjean, R.E. Benfield, E. Olsson, K. Niihara, L.R. Wallenberg, Chem. Mater. 14 (2002) 3686.
[47] P. Ratnasamy, D. Srinivas, C.V.V. Satyanarayana, P. Manikandan, R.S.S. Kumaran, M. Sachin, V.N. Shetti, J. Catal. 221 (2004) 455.
[48] G. Wrobel, C. Lamonier, A. Bennani, A. Aboukais, J. Chem. Soc., Faraday Trans. 92 (1996) 2001.
[49] R.G. Ranga, S.H. Ranjan, M.B. Gopal, Colloids Surf. A 220 (2003) 261.
[50] A. George, I. Theophilos, Appl. Catal. A 244 (2003) 155.
[51] X.L. Tang, B.-C. Zhang, Y. Li, Y.-D. Xu, Q. Xin, W.-J. Shen, Catal. Today 93–95 (2004) 191.
[52] A.G. Knapton, Plat. Met. Rev. 21 (1977) 44.
[53] F.R. Garcia-Garcia, M.A. Rahman, B.F.K. Kingsbury, K. Li, Catal. Commun. 12 (2010) 161.
[54] D.T. Hughes, I.R. Harris, J. Less Common Met. 61 (1978) 9.
[55] D. Wang, T.B. Flanagan, K.J. Shanahan, J. Phys. Chem. B 112 (2008) 1135.